Measurements of Electrical Resistivity Index of Tight Gas Sandstones Using Vapor Desorption Method, Nuclear Magnetic Resonance, and Corrections for Effect of Clay Conductivity, Salinity and Density Change.

Dhafer Badhafere[1], Abdulrauf R. Adebayo*[1], Jun Gao[2], Hyung Kwak[2], Abdullah Alkhaldi[2], Abdul-Qadir Mohammed[2], Khaled Z. Ibrahim[1], Ammar H. ElHusseiny[1], Gabor Hursan[2], and Mohamed Mahmoud[1]

[1]College of Petroleum Engineering and Geosciences, King Fahd University of Petroleum & Minerals, Saudi Arabia.
[2]Exploration and Petroleum Engineering Center – Advanced Research Center, Saudi Aramco, Saudi Arabia.

Abstract. The measurement of electrical resistivity in tight sandstone cores, characterized by low permeability (0.01 – 0.1mD) presents significant challenges such as the need for a high capillary desaturation method which cannot be attained with a conventional porous plate method, a small pore volume that can make the estimation of water saturation susceptible to error, and the presence of clay minerals. The vapor desorption method can desaturate the cores at higher capillary pressures, but it is also faced with some challenges such as changing brine salinity, changing brine density, and salt precipitation, which affect the resistivity index curve and the determination of saturation exponents. This study aims to develop a reliable workflow for measuring electrical resistivity in tight sandstone cores with a vapor desorption technique while addressing these challenges. Some tight sandstone cores (permeability: 0.01mD to 0.05mD, and porosity: 5-10%), were carefully cleaned using a benign solvent extraction method to protect the clay fabrics. The samples were then saturated with brine, with full saturation confirmed when gravimetric porosity matched helium porosity. A porous plate capillary desaturation was first conducted up to a maximum pressure of 200psi, where no brine was displaced from the samples. A humidity oven was then used to impose relative humidity starting from 95% and then decreased stepwise to 90%, 85% and 70% with corresponding capillary pressures of 1000 psi up to 7203 psi, to achieve different water saturations. Electrical resistivity was measured at each saturation point, and the corresponding resistivity index values were estimated. Two empirical models were derived from a separate desorption experiment on bulk brine to correct for resistivity and salinity changes during the vapor desorption experiments, after which the true resistivity index plots were obtained and then the correct saturation exponents obtained. Multi-salinity test was also conducted on the samples to correct for the effect of clay conductivity on the saturation exponent. Finally, a correlation between true resistivity index and NMR T_2 was developed to allow for fast estimation of electrical properties. This paper summarizes the comprehensive workflow for determining electrical resistivity indices in tight gas and offers procedures for addressing and avoiding related challenges, such as salt crystallization during desaturation.

1 Introduction

Considerable data must be obtained from core and log data to adequately evaluate tight sands. An important parameter required in the volumetric calculation is the connate water saturation normally obtained from log and/or core data. Special core analysis must be conducted on selected core plugs extracted from tight reservoirs to obtain connate water saturation and other high quality petrophysical data such as porosity, permeability, resistivity index, formation factor, capillary pressure, clay bound water, and capillary bound water [1-3].

Accurate measurement of these rock properties is essential for evaluating reservoir rocks, particularly low porosity,low permeability rocks such as tight gas sands [4]. Petrophysical measurements and interpretations in such rocks are quite challenging because of many factors: the presence of small unconnected pores, accessory minerals, clay swelling, fines migration, gas slippage effect, and turbulence [5], [6], [7]. It is essential to preserve clay structure during sample preparation and petrophysical studies such as electrical resistivity, capillary pressure, and permeability measurements.

For water saturation estimation, the Archie model [8] and its modifications [9] as shown in Eq. 1-2 are commonly used to estimate water saturation from electrical resistivity logs in conventional reservoirs. The model parameters (saturation exponents, cementation factor, and tortuosity factor) are obtained from electrical resistivity

* Corresponding author: abdulrauf@kfupm.edu.sa

measurements of representative core plugs. Clay (when present) also adds extra conductivity to the rock which can result in overestimation of water saturation. With the presence of clay and high-density materials (such as pyrites and hematite), the conductivity of such rocks is not only caused by the saline water in them but also by some rock minerals. This phenomenon is common in shaly rocks, with significant clay content. Several modifications of the Archie model have thus been developed to accommodate more heterogeneous and complex rock systems such as sandstones with clay and other conductive minerals. These modifications include those by Waxman and Smits [10], the Indonesian model [11]; and the Simandoux model [12]. The workflow to measure resistivity model parameters in conventional reservoirs has been available for many decades and well-established. However, there is currently no universally accepted workflow to measure saturation exponent for tight rocks. This is largely due to the very low permeability and complex pore geometry which make the conventional porous plate and centrifuge methods impossible or inadequate.

$$F = \frac{R_o}{R_w} \tag{1}$$

$$S_w = \left(\frac{R_0}{R_t}\right)^{1/n} = \left(\frac{1}{RI}\right)^{1/n} \tag{2}$$

$$F = \frac{a}{\phi^m} \tag{3}$$

$$S_w = \left(\frac{aR_w}{\phi^m R_t}\right)^{1/n} = \left(F\frac{R_w}{R_t}\right)^{1/n} \tag{4}$$

Where F is the electrical formation factor, R_o is the electrical resistivity of a rock fully saturated with formation water, R_w is the electrical resistivity of the formation brine, S_w is water saturation in the rock, R_t is the true resistivity of formation, RI is the resistivity index ($RI = \frac{R_t}{R_o}$), and n is the saturation exponent.

These equations work well in clean and non-conductive clastic rocks. The parameters (a, m, n) are often derived through a standardized laboratory workflow using porous plate or centrifuge methods [13], [14], [15]. Such measurements produce resistivity of a rock sample at different partial water saturations. The slope of the log of resistivity index ($\frac{R_t}{R_0}$) versus the log of water saturation (S_w) produces the saturation exponent (n) while the slope of the log of formation factor (F) versus the log of porosity (ϕ) yields the cementation exponent (m). The intercept of $F - \phi$ plot at a porosity value of 100% is the tortuosity factor (a).

Low permeability sands have very small pores with a large surface area to volume ratio. Consequently, adsorption and capillary condensation significantly contribute to high water retention at a corresponding extremely high capillary pressure in these rocks [16]. Some low permeability sands have ultra-low saturation at extreme capillary pressure, probably as a result of the water vaporization process caused by the flow of dry hydrocarbon gas through the rock [17]. Strong adhesive forces hold the wetting film (water) that covers the rock surface while capillary forces hold the bulk water phase in place with a curved interface separating the water and gas/vapor phase. The partial pressure of the vapor in equilibrium with the bulk liquid is a function of the interfacial curvature [18]. Young-Laplace equation (Eq. 5) shows that capillary pressure is also a function of the liquid-vapor interfacial curvature. Since the interfacial curvature between vapor and liquid is dependent on the saturation of the liquid phase, it then follows that partial pressure and capillary pressure are dependent on the saturation of the liquid [17], [18]. Hence, a relationship between capillary pressure and vapor pressure was derived [16], [17], [18], [19], [20]. The general form of the relationship in terms of partial pressures is given by equation (6), while equation (7) shows the equation rewritten in terms of relative humidity.

$$Pc = \frac{2\sigma}{r} \tag{5}$$

$$Pc = ln\left(\frac{P_{v1}}{P_{v2}}\right)\frac{RT}{V_m} \tag{6}$$

$$Pc = -\frac{\ln\left(\frac{RH}{100}\right)RT}{V_m} \tag{7}$$

Where Pc is capillary pressure in psi, σ is the interfacial tension in pounds per inch, r is the radius of curvature in inches, P_{v1} is the partial vapour pressure for brine within the pores, P_{v2} is the partial vapour pressure for equilibrating salt solution, R is the universal gas constant, 8.314 J/mol.K, T is absolute temperature in kelvins, V_m is the molar volume of water, RH is the relative humidity of water vapour in percentage that could be deduced from equation 8.

$$RH = \left(\frac{P_{v1}}{P_{v2}} \times 100\right) \tag{8}$$

Equations 5 and 6 are referred to as the modified Kelvin equation, originally derived by Thomson [1871], which is a model that gives a relationship between change in vapor pressure (or relative humidity) and capillary pressure. Hence, the reduction in the vapor pressure of a gas-liquid porous medium (vapor desorption) can be used to calculate capillary pressure using Equations 5 or 7. It was later shown that vapor-desorption data can be used to derive capillary pressures in low permeability reservoir rocks [16], [17], [18], [19], [20].

The Kelvin equation is valid for all saturation ranges but mostly applicable for low saturation range, where water saturation is reduced to water films adsorbed on rock grains. At such ultra-low water saturation, the water is held in place by adhesive forces corresponding to an extreme capillary pressure. The Laplace equation is more applicable at higher liquid saturation, where there is a clear interfacial curvature between the liquid and vapor phase. A conceptual model that illustrates the transition between water held by adsorption (sub-capillary equilibrium) and water held mainly by capillarity and the applicable capillary pressure model was provided by Newsham et al., [2003] [17] as shown in Fig. 1.

As shown by Equation (7), the capillary pressure of rocks can be computed by lowering the vapor pressure in a humidity or relative humidity chamber.

The main advantage of the vapor desorption method is the ability to obtain very high capillary pressures and consequently desaturate tight reservoir rocks. Vapor desorption method was used to measure the capillary pressures of a Bossier tight gas sand (with permeability range of 0.0006 mD to 0.14 mD). High speed centrifuge measured capillary pressure in the range of 14 bar to 55 bar, while the vapor desorption method measured capillary pressure in the range of 14 to 700 bar [16], [22]. It was shown that vapor desorption capillary pressures agree well with high-speed centrifuge capillary pressures (in the range of 14 bar to 55 bar). Vapor desorption method has also been used to measure capillary pressure at different water saturations and the corresponding electrical resistivity of tight rock samples at different partial water saturations [23], [24]. Both drainage and imbibition can also be conducted with vapour desorption method. However, vapor desorption method can only be used for rocks whose permeability is extremely low. Applying this technique on a rock whose permeability is not sufficiently low can lead to complete desaturation even at a high relative humidity of 95%. Another disadvantage of the vapor desorption method is the extensive time required to achieve equilibrium. It can take days to weeks to achieve equilibrium in each saturation or relative humidity step [17], [23], [24]. It is therefore helpful if a model is developed based on experimentally derived data to predict resistivity index from some measurable pore attributes. Another challenge when dealing with vapor desorption is liquid evaporation where brine concentration would increase due to liquid phase evaporation leading to fluctuations in resistivity readings that can affect conventional applications of Archie's equation. The effect of active clay conductivity can also come into play at low brine concentrations leading to changes in resistivity and formation factor, which requires further correction.

Several predictive methods have also been developed to predict the saturation exponent. Famous among them is NMR based models. The NMR based model is an indirect method based on statistical correlation between measured NMR T_2 data and measured electrical resistivity data. Xiao et al. [2013][25] reported a correlation between saturation exponent (n), the logarithmic mean of the NMR T_2 relaxation time (T_{2LM}), irreducible water saturation, and resistivity index.

Xiao et al. [26] later correlated electrical resistivity with T_{2LM}. Feng et al. [27] gave a more detailed correlation between electrical resistivity index and several petrophysical properties of rocks such as T_{2LM}, porosity, permeability, and capillary pressure. This study presents a workflow to measure Archie parameters (a, m and n) for very tight gas sandstone formations using vapor desorption as the main technique and discusses the major challenges with that technique. In addition, NMR data are correlated with resistivity data to study the applicability of NMR in providing a robust method to predict Archie parameters for tight gas sandstones.

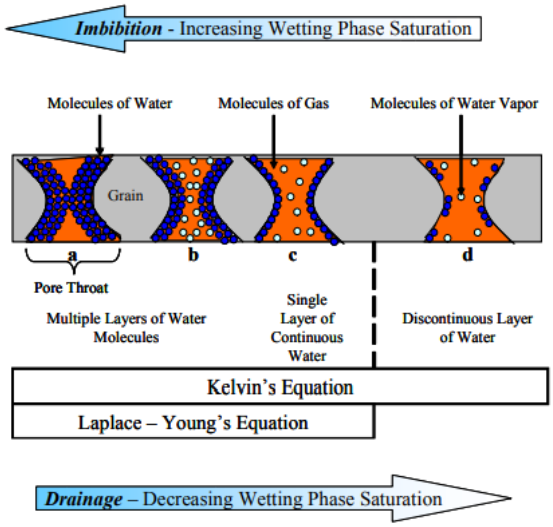

Fig. 1. A conceptual model illustrating transition between capillary held water phase and water trapped at sub-capillary equilibrium state. Also shown is the applicable capillary pressure models [17].

2 Samples and Experimental Procedure

Samples from an Arabian tight gas sand were received along with their preliminary data. Once received, the samples were measured for dimensions and weights. **Table 1** illustrates the dimensions of the core samples. Sample surfaces were also checked to ensure their fitness for electrical resistivity measurements. Surface flatness is responsible for the quality of the electrical signal in contact with the rock surface. To ensure good electrical contact with the samples, brine-wetted fiberglass filters were placed at the contact with the current electrodes.

Table 1: Samples dimensions

Well	A	B	C	C	D
Sample No.	**1**	**2**	**3**	**4**	**5**
Dry weight (g)	178.68	159.96	178.64	126.93	178.68
Length (cm)	6.80	6.19	6.35	4.91	6.80
Diameter (cm)	3.73	3.78	3.78	3.74	3.73

2.1 Samples preparation

To ensure the samples were cleaned of any contaminants, they were placed in a hot solvent cleaning rig for several days to clean any residual materials inside the cores. After cleaning, samples were vacuum-dried for several days until weight stabilization was achieved within 0.01 g accuracy. Then the cores were set for saturation. In this stage, the cores are placed in a sealed cell and vacuumed for several days. After vacuuming, the cores were saturated with 3 wt.% KCl brine under a 2,000-psi applied pressure for several days. The brine is of 1.0162 g/cc density and 0.19 ohm.m resistivity. Saturating

at such high pressures assures that the samples were well-saturated and that most of the effective pores were filled.

2.2 Samples petrophysical data

The cores' primary petrophysical data were measured in both dry and saturated conditions. The petrophysical data are summarised in **Table 2**. Saturated core samples were set for multiple porosity checks due to the nature of the samples having low permeability. In this stage, porosity was measured using two effective methods that are matched to insure accurate measurements i.e., helium porosity as the primary method and NMR porosity as supportive validation method. Helium porosity was confirmed with NMR porosity results which ensures correct measurements and full saturation of the core samples. The measured NMR porosity shows a good match with the provided helium porosity with an error margin of ±0.5% (shown by the dotted lines in **Fig. 2**) which indicates a successful saturation procedure. XRD data shows a dominant quartz composition; however, some cores have traces of heavy metals and clays at low concentrations as shown in **Table 3**.

2.3 Experimental methodology

Core samples were desaturated in two stages: porous plate desaturation and vapour desaturation. First, fully saturated core samples are desaturated via porous plate in a closed chamber under various levels of capillary pressure from 50 to 189 psi to facilitate brine desaturation.

Saturation values were monitored. Once the fluid discharge was stable, electrical resistivity was measured and then used to calculate the resistivity index for the estimation of the saturation exponent. **Fig. 3** illustrates the processes conducted in the porous plate desaturation.

In vapor desaturation, samples are transferred to the humidity oven. In this stage, the aim is to exert descending humidity levels on the core samples that are equivalent to certain capillary pressure values at a constant temperature following **Equation 7**. A humidity oven from Memmert was used at a fixed temperature of 35° C and humidity levels of 95%, 90%, 85% and 75%. At each stage, the core samples were checked continuously for weight stability and electrical resistivity measurements were done once the weights of the core samples were stable. **Fig. 4** shows the methodology of the vapor desaturation stage.

Table 2. Samples petrophysical properties

Well	A	B	C	C	D
Sample No.	**1**	**2**	**3**	**4**	**5**
Helium Porosity (%)	10.21	12.17	5.84	5.33	10.35
Gas Permeability (mD)	0.038	0.04	0.024	0.047	0.072
Pore Volume (cc)	8.01	8.68	4.26	3.58	5.79
Grain density (g/cc)	2.65	2.68	2.65	2.65	2.64

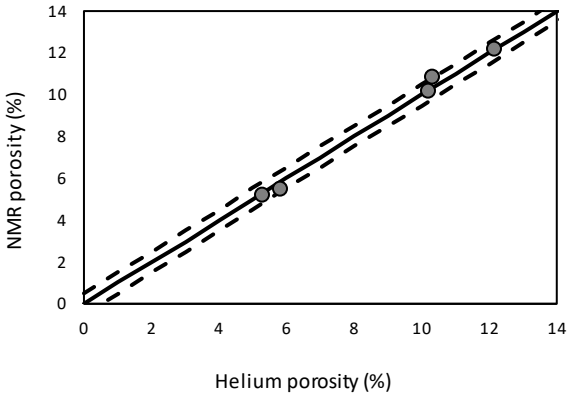

Fig. 2. NMR porosity as a confirmation method to helium porosity. The broken lines are the ±0.5% error margin.

Table 3: XRD analysis for the set of samples

Well	A	B	C	C	D
Sample No.	**1**	**2**	**3**	**4**	**5**
Clays (wt. %)	0	1.7	0	1.1	0
Heavy metals (wt. %)	1	2	0.0	0	0
Carbonates (wt. %)	3.3	6.2	1.2	0.8	13.1
Quartz (wt. %)	95.2	89.3	98.1	97.3	83.5

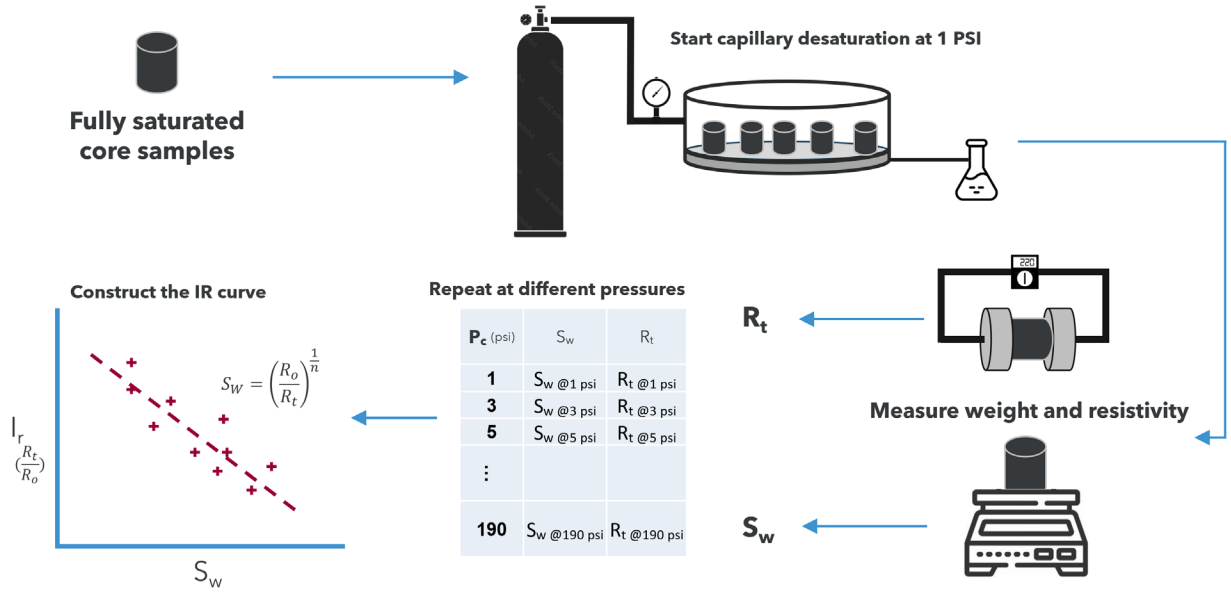

Fig. 3. Porous plates experimental procedure

3 Results and discussion

3.1 Formation factor and clay effect

The electrical resistivity of the samples was measured at 1 kHz using both at 2-pole and 4-pole. **Fig. 5** illustrates the cross plot of electrical formation factors versus porosity for the studied set of core samples. The values of a and m are obtained by fitting the data to a power law correlation and the value of a is found to be 5.4 while that of m is 1.3 (for a 2-pole measurement). If the data are forced-fitted with Archie's model such that the value of a is set to 1, then the values of m align around 2 for all the samples. The tests were repeated after about a month interval to ensure repeatability of measurements and the results showed that the 2-pole configuration was repeatable with a maximum tolerance of 1.5 ohm.m while the 4-pole is repeatable with a maximum tolerance of 3 ohm.m.

The tortuosity factor (a) for this tight sandstone is quite high (a = 5.4). Such high values were reported in some published studies on tight sandstone. Xiao et al. [25] reported various high values of tortuosity factor for different wells such as 3.63, 4.43, and 4.87 for core plugs with a porosity range of 1.3 to 21.8% and permeability of 0.01 to 825 mD. Adebayo et al. [3] also reported a tortuosity factor of 5.14 for some rock samples from Sarah sandstone formations.

The existence of clays can hinder the accuracy of resistivity studies. Clays can impact the resistivity readings for their conductive nature. Active clay conductivity can affect the measured electrical resistivity by reducing it below the actual value, leading to underestimated R_t value that affects both formation factor and saturation exponent estimations. One way to qualitatively identify the effect of active clay conductivity is electric formation factor. Moreover, the effect of clay conductivity weakens as brine salinity increases, which is a key indicator of that effect.

Active clay conductivity interference is studied in a multi-salinity process. The core samples were saturated in higher brine concentration i.e., 20 wt.% KCl. Electrical resistivity was measured and the formation factor was calculated. Formation factor at 3 wt.% KCl and 20 wt.% KCl were calculated for the core samples and plotted against each other in a cross plot to see the effect of clays. **Fig. 6** shows that the formation factor is diverging from the unity line with higher values for the 20 wt.% KCl. While this can be attributed to active clay conductivity, other factors such as porosity, heavy metals, and semiconductors (i.e., pyrite) can play a role in that divergence. As seen in **Fig. 7**, higher divergence is shown in lower porosity cores while the divergence is low in higher porosity cores. Other contents' effect was studied as well i.e., heavy metal content (**Fig. 8**) and pyrite content (**Fig. 9**).

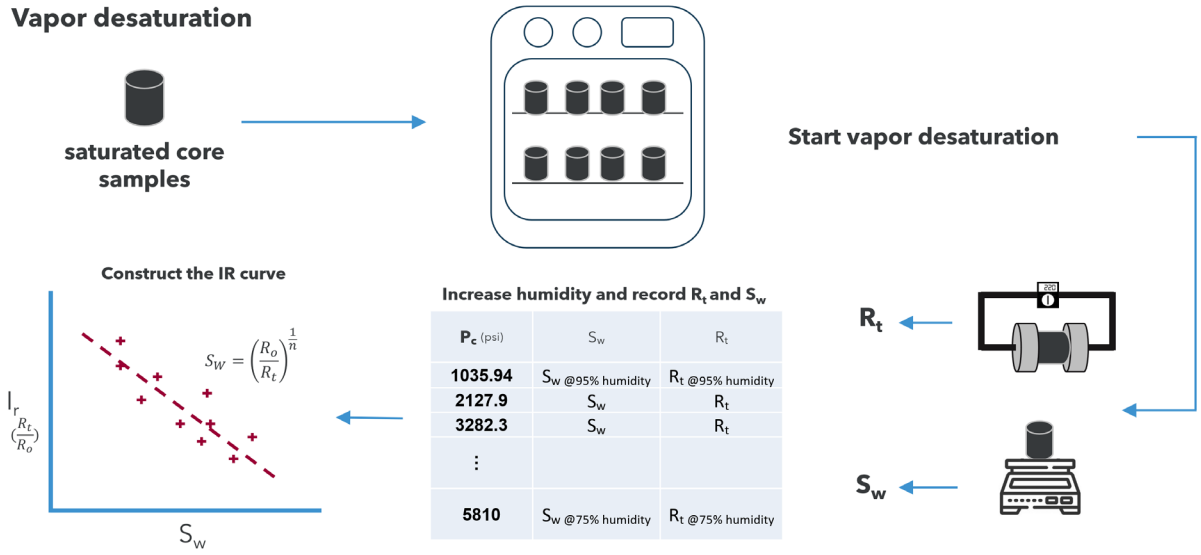

Fig. 4. Vapor desorption stage experimental procedure

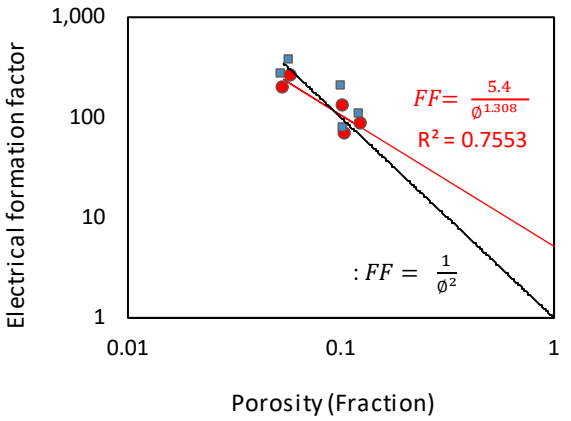

Fig. 5. Electrical formation factor (with 20% KCl) versus porosity and Archie parameters estimation (a and m)

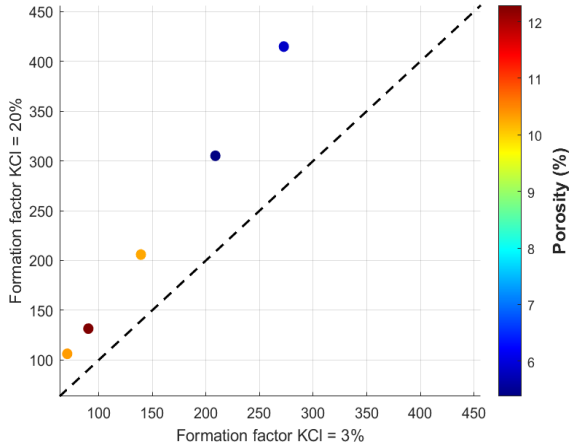

Fig. 7. Electric Formation Factor at different KCl salinities with porosity

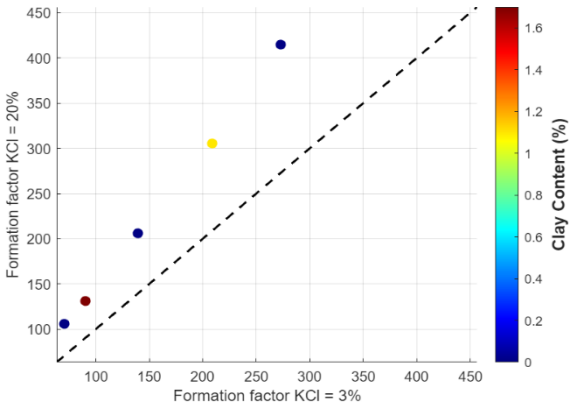

Fig. 6. Electric Formation Factor at different KCl salinities with clay content

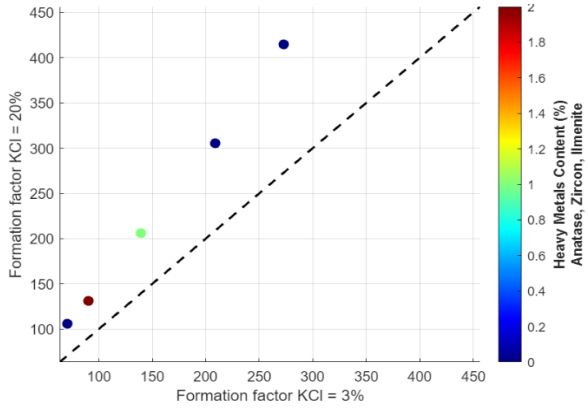

Fig. 8. Electric Formation Factor at different KCl salinities with heavy metals content

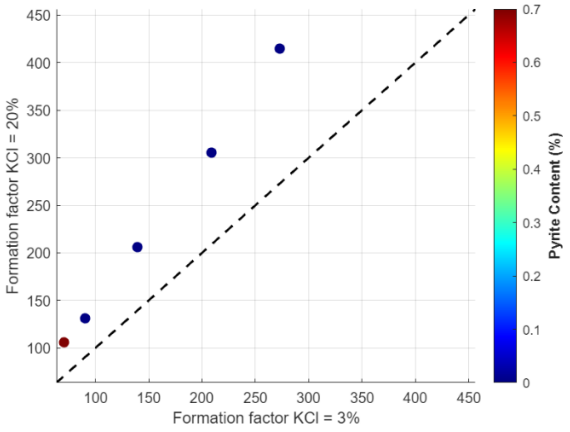

Fig. 9. Electric Formation Factor at different KCl salinities with pyrite content

3.2 Saturation exponent without correction

In the initial stages, fully saturated core samples are desaturated via porous plate in a closed chamber under various levels of capillary pressure to facilitate brine desaturation. In this stage, a starting pressure of 50 psi is used followed by 100 psi then 150 psi reaching to 189 psi, where the limit of the porous plate is 200 psi. Saturation values are monitored once the fluid discharge is stable and electrical resistivity is measured and used to calculate the resistivity index and estimate the saturation exponent. Most of the core samples are tight ranging from 0.024 to 0.072 mD. This requires higher pressure values to desaturate the core samples. At the beginning of the desaturation stages at 50 psi capillary pressure, no significant reduction in saturation was observed, and resistivity remained close to initial values. As pressure increased, minor changes in brine saturations were observed which were insufficient to produce data points for constructing a meaningful plot in the resistivity index plot. **Fig. 10** shows core weights post porous plate desaturation indicating minimal brine loss. Most cores retained over 90% saturation. Hence, the second stage of desaturation — vapor desaturation — was initiated.

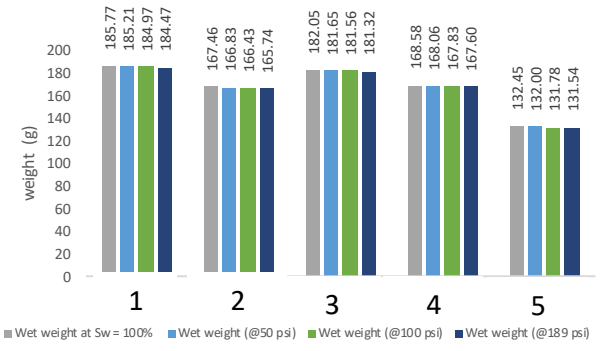

Fig. 10. Weight difference during porous plates stage

The vapor desaturation process began after the porous plate desaturation phase where the samples were transferred to the humidity oven. In this stage, the aim is to exert descending humidity levels on the core samples that are equivalent to certain capillary pressure values at a constant temperature following **Equation 7**. A humidity oven from Memmert was used at a fixed temperature of 35° and humidity levels of 95%, 90%, 85% and 70%. At each stage, the core samples are checked continuously for stability and electrical resistivity measurements are done once the wrights of the core samples are stable and no longer decreasing due to desaturation.

At first, the samples were put at 95% relative humidity and weight was monitored over the testing period. Clear and effective desaturation took place with core samples saturation levels dropping below 50% for most samples (**Fig. 11**). Such desaturation influenced increasing resistivity values in the core samples. Electric resistivity was monitored for the core samples after each stage, starting at 95% relative humidity, that is equivalent to 1035.94 psi. As seen in **Fig. 12** resistivity values have increased significantly due to the desaturation that took place.

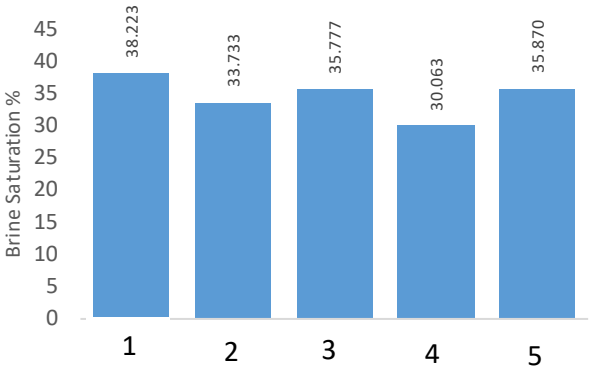

Fig. 11. Samples Saturations after 95% relative humidity

Afterwards, desaturation resumed at lower humidity levels, 90%, 85%, and 75%, which are equivalent to 2127.9, 3282.3, and 5810.1 psi respectively. At each stage, the saturation levels continued to decrease, and electrical resistivity was increasing accordingly. **Fig. 13** shows an example of one core sample desaturation profile with electric resistivity.

Desaturation profiles for each core sample were achieved from the desaturation process which were used to analyze and model saturation exponent plots. For each core sample and at each step, the resistivity index was calculated by dividing the current resistivity reading, R_t, by the initial reading at 100% brine saturation, R_o, considering in this case Ro as the constant resistivity of the saturating fluid. Log values of resistivity index values are plotted against log values of the saturation laying the resistivity index profile of the core sample. The log-log relation reveals a trend that can be represented by an equation where n, the saturation exponent, is the slope. **Figures [14-18]** present the results for the tested set of samples.

Saturation exponent values are observed to be lower than expected for these tight sandstones where it has been reported in earlier research to be around 1.4 to above 7

depending on the composition of the samples, permeability, porosity system and many other petrophysical properties that can directly affect saturation exponent [28], [29]. The main reason in the current case is suggested to be the change in salinity of brine during vapor desaturation causing R_o to decrease with the evaporation of water, resulting in relatively lower RI values and, consequently, flatter and underestimated n values. In the next subsection, the effect of salinity change is studied and corrected.

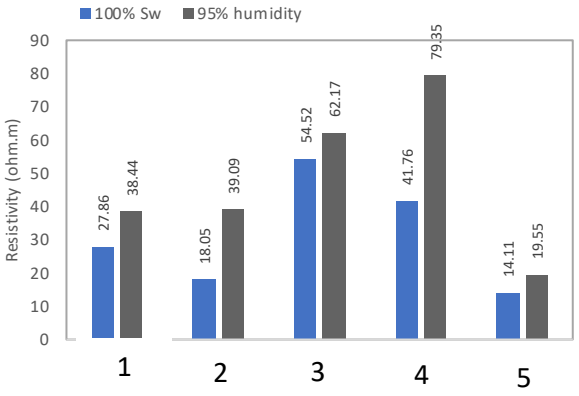

Fig. 12. Resistivity difference at 95% relative humidity

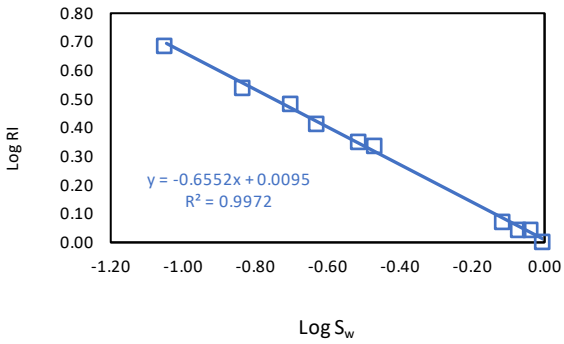

Fig. 13. Resistivity profile for sample B (2)

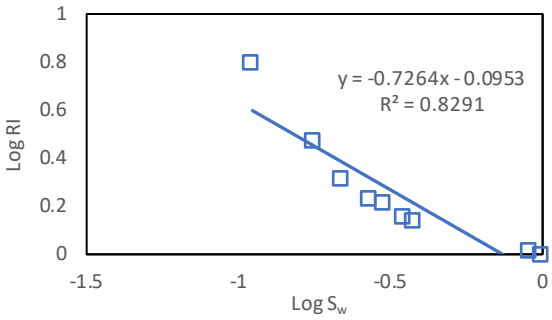

Fig. 14. Resistivity index profile sample A (1)

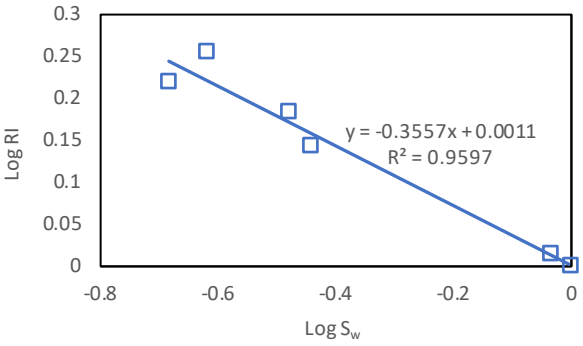

Fig. 15. Resistivity index profile sample D (5)

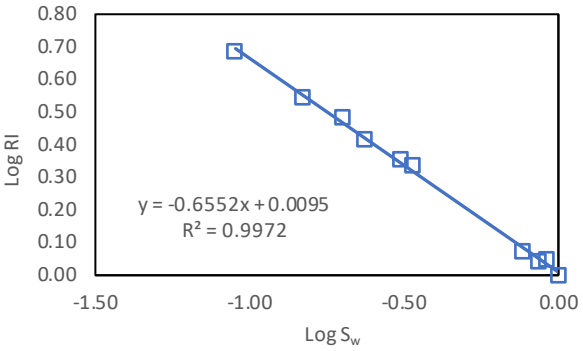

Fig. 16. Resistivity index profile sample B (2)

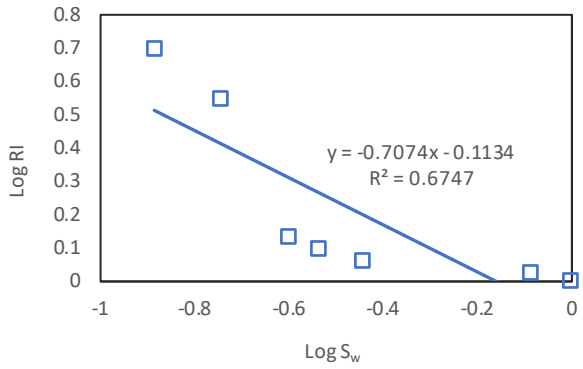

Fig. 17. Resistivity index profile sample C (3)

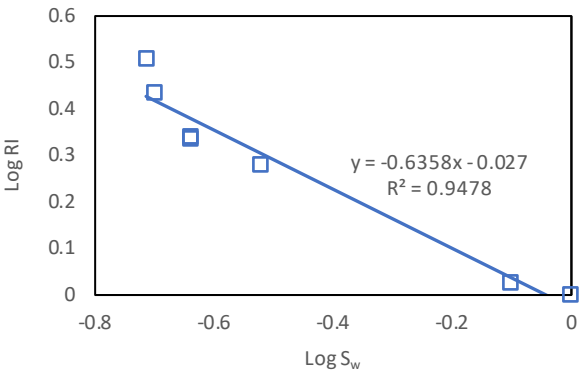

Fig. 18. Resistivity index profile sample C (4)

3.3 Correction for Salinity, clay, and density effect

The nature of vapor desaturation depends on desaturating the core samples by applying humidity ranges to a sealed environment. This procedure causes the liquid saturating the core samples to evaporate, while the salt remains in the fluid, increasing its concentration, as seen in **Fig. 19**. The increase in concentration leads to changes in electric resistivity values, resulting in lower R_t readings due to higher brine conductivity. In addition, a critical effect is the change of the R_o value. For the resistivity index relation ($RI = \frac{R_t}{R_o}$) to be meaningful, the value of R_o needs to remain constant as initially measured at full brine saturation, ensuring the RI remains a valid ratio between the partially desaturated case, and the fully saturated case.

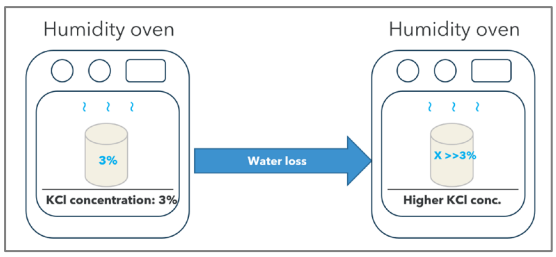

Fig. 19. Concentration increase due to liquid evaporation

However, in this case having a positive change in brine concentration will affect the brine electric resistivity and lower the resistivity values of R_t, while R_o is assumed to be constant and thus overestimated compared to the its actual value under changing concentration. This leads to inaccurate estimations of both resistivity index and saturation exponent. Moreover, the density is expected to increase due to loss of liquid phase, making the fluid relatively denser which directly affects the saturation. To study the effect of density, change on saturation, bulk fluid multi-salinity test is conducted to establish a relationship between density and concentration of KCl brine (**Fig. 20**). Brine density was measured with a densitometer.

$$Density\ (g/cm^3) = 0.681 * Concentration^{0.9949} \quad (9)$$

Saturation is calculated by dividing the pore volume by the fluid volume obtained from equation 10.

$$V_f = \frac{m_f}{\rho_f} \quad (10)$$

Where m_f is the mass of the fluid and ρ_f is the density obtained from equation 9.

Density and saturation at each current stage were calculated from the concentration in an iterative method until the values converge. It has been found that the effect of density increase is minimal on saturation values. A sensitivity analysis was conducted on one of the core samples to see the effect of a wide range of density changes on saturation (**Fig. 21**). Broad changes in concentrations would result in minor changes in density and saturations that can be estimated at an increase of 0.03405 g/cm^3 in density and 0.0109 decrease in saturation. When applied to one core sample, no considerable variation in the value of saturation exponent was obtained as shown in **Fig. 22**.

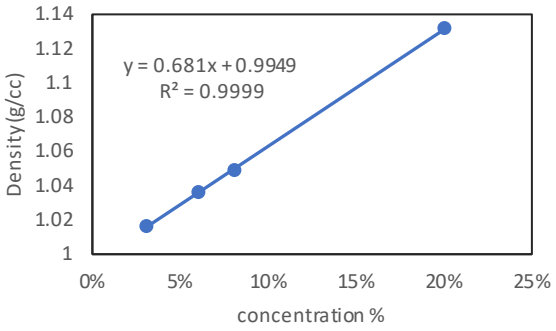

Fig. 20. Brine density as a function of concentration

To correct for the brine concentration effects, R_o values need to be updated dynamically at each saturation step. This involves adjusting the concentration and using a more accurate Ro value for calculating RI and saturation exponent estimation. A process of analytical and mathematical steps is introduced to correct for R_o values due to desaturation and concentration change. The correction process starts with the estimation of brine concentration by concentration conservation relation show in equation 11.

$$C_i V_i = C_f V_f \quad (11)$$

Where C_i is the initial concentration, V_i is the initial volume, C_f is the final concentration and V_f is the final volume. The volume can be deduced from the saturation where $V_f = S_w * PV$. Second, the relation between core resistivity at 100% brine saturation and brine concentration needs to be established. Each core sample is saturated with brines of varying concentrations, and R_o values are recorded. The values will be used to construct the plot in **Fig. 23**. The plot establishes the relation between brine concentration that is currently saturating the core samples, and its Ro value that should be used in the resistivity index relation to yield accurate results. After concentration from equation 11, Ro is estimated from the chart in **Fig. 23** and correct RI values are calculated to be plotted for estimation of n values. After correction, the RI— saturation plot changed in form.

After applying the correction scheme, there have been clear improvements to the saturation exponent values and resistivity index profile with desaturation. The values of n increased and the effect of salinity change was mitigated by dynamically changing R_o to its concentration-corresponding value. **Figures [24-28]** show the corrected saturation profiles.

Clay effect can be corrected by multi-salinity test, in which the core samples are saturated with brine of varying salinities to establish a plot of core conductivity versus brine conductivity. By plotting fluid and rock conductivity, a straight line can be extrapolated with its slope representing the reciprocal of the intrinsic electrical

formation factor FF^* (**Fig. 29**). Intrinsic Archie parameters are then calculated by plotting FF^* versus porosity.

Moreover, intrinsic saturation exponent can be estimated from a plot of intrinsic resistivity index (RI) versus water saturation on a log-log scale, where RI^* can by calculated using **Equation12**. The parameter B is calculated using **Equation 13,** as presented by Dacy and Martin [30] and Q_v is deduced from the y-intercept of the core conductivity versus brine conductivity plot.

$$RI^* = RI\left[\frac{1+\frac{BQ_vR_w}{S_w}}{1+BQ_vR_w}\right] \quad (12)$$

$$B = \left[1 - 0.83exp\left[-\frac{\left[-2.47+0.229ln(T)^2+\frac{1311}{T^2}\right]^{-1}}{R_w}\right]\right](-9.2431+ 2.6146T^{0.5}) \quad (13)$$

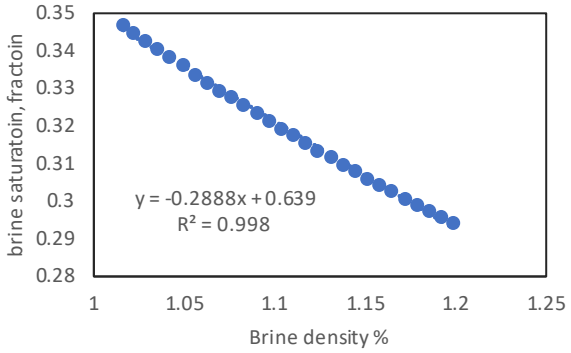

Fig. 21. Effect of brine density on saturation levels

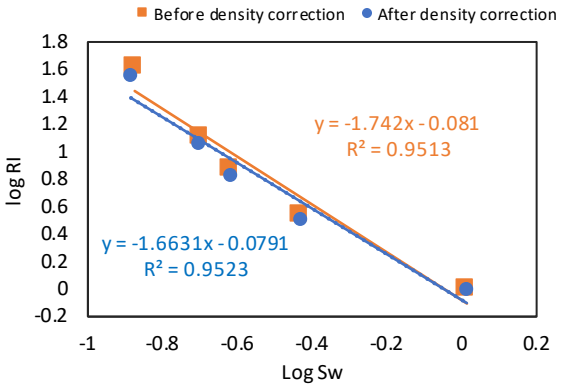

Fig. 22. Effect of density change on saturation exponent

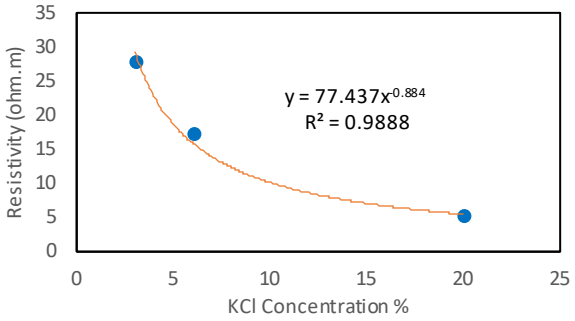

Fig. 23. Resistivity correlation with KCl brine concentration

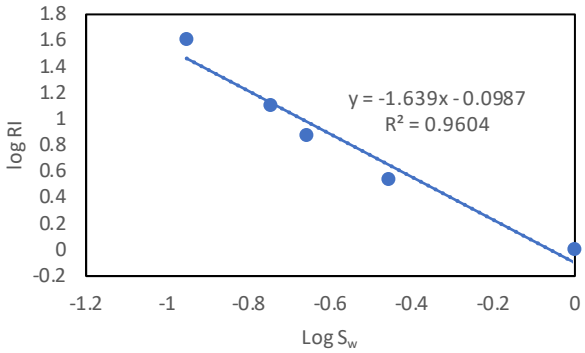

Fig. 24. Corrected resistivity index profile sample A (1)

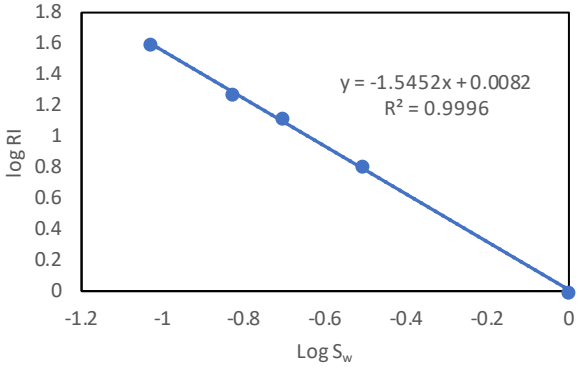

Fig. 25. Corrected resistivity index profile sample B (2)

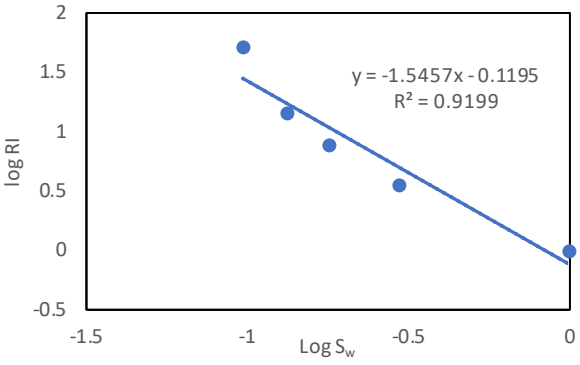

Fig. 26. Corrected resistivity index profile sample C (3)

Comparing the corrected tortuosity factor (*a*) and cementation factor (*m*) to the initial value before correction, the tortuosity factor (*a)* increases from 5.14 to 7.9 while cementation factor m increases from 1.31 to 1.37, indicating the influence of active clay conductivity at low brine salinity. **Table 4** summarises the changes in *a, m*, and *n* after clay correction for clay and salinity.

Table 4: summary of *a, m*, and *n* before and after corrections.

	Before correction	After correction
a	5.4	7.9
m	1.31	1.37
n		
A1	0.726	1.639
B2	0.655	1.545
C3	0.707	1.546
C4	0.636	1.898
D5	0.356	1.59

3.4 NMR to predict Archie parameters

NMR relaxation time T_2 can be used to predict Archie parameters by correlating T_2 relaxation times of core samples with resistivity index calculated from the conventional desaturation process [26]. In this study, NMR T_2 times are correlated with the corrected resistivity index (from section 3.3) to establish a correlation that can be applied locally to reservoir rocks with comparable petrophysical properties. T_2 distribution was converted to T_2-Sw distribution by normalizing the T_2 – cumulative porosity such that the porosity transforms to a water saturation scale (from 0 – 1). This allows T_2 values to be mapped with the corresponding resistivity index at the same water saturation as shown in **Fig. 31**. The correlation is later used to predict the resistivity index at any saturation state within the used range, hence allowing for prediction of the saturation exponent from the resulting resistivity index profiles. Nevertheless, the complexity of very tight gas sandstones makes it difficult to apply the correlation across other samples due to differences in composition, pore system and permeability. **Figure 32** shows a typical T_2 distribution at different saturations.

4 Conclusions

In this study, a comprehensive workflow is presented to estimate Archie parameters for tight gas sandstones using the vapor desorption method. Salinity change, a major challenge in vapor desorption method, was addressed by applying a dynamic resistivity correction method that led to more accurate prediction of saturation exponent. Cementation factor and tortuosity factor were estimated and corrected for clay presence that disturbs the resistivity readings due to active clay conductivity. Correction was done by acquiring intrinsic properties from core/brine conductivity plots. NMR data were correlated with resistivity index in pursuit of achieving a local correlation that can predict saturation exponent directly from NMR T_2 data. Although the correlation was reached successfully, it was not applicable across other samples due to differences in composition, petrophysical properties and pore system that affect NMR measurements, hence affecting the correlation outcomes.

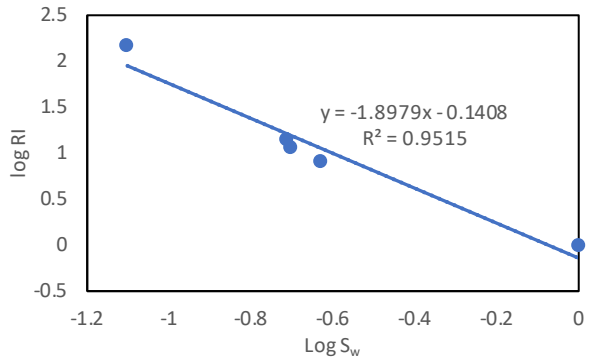

Fig. 27. Corrected resistivity index profile sample C (4)

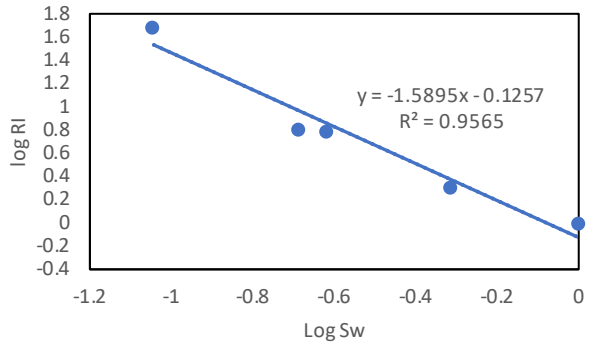

Fig. 28. Corrected resistivity index profile sample D (5)

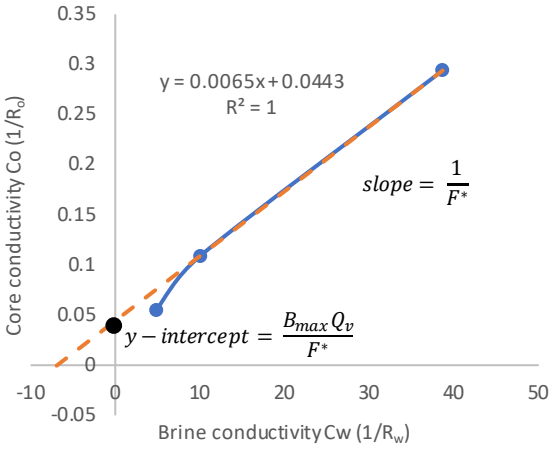

Fig. 29. Core conductivity versus brine conductivity to establish intrinsic properties for sample B (2)

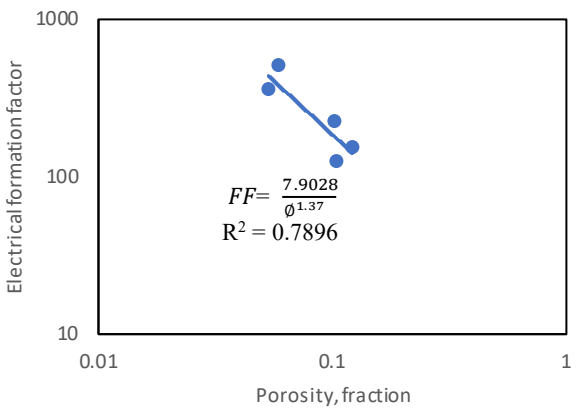

Fig. 30. Intrinsic electrical formation factor versus porosity to obtain *a* and *m*

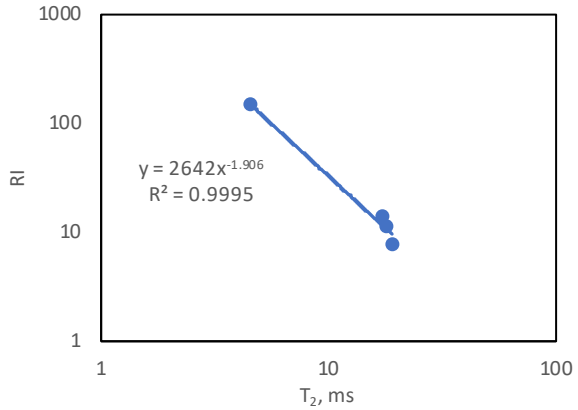

Fig. 31. Resistivity index correlation with NMR T_2

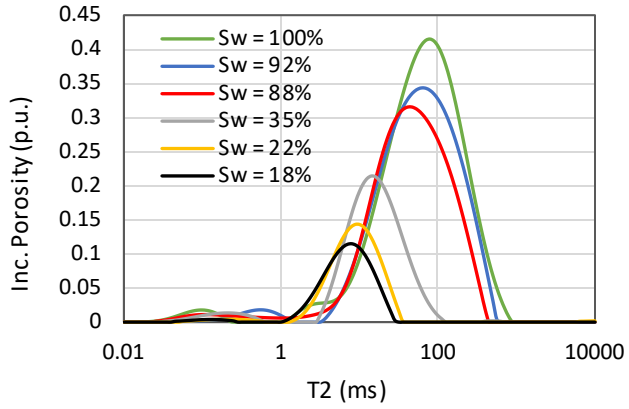

Fig. 32. T_2 distribution at different saturation for sample A (1)

References

1. Holditch, S. Tight Gas Sands. *J. Pet. Technol.* **58**, 86–93 (2006).
2. Soeder, D. J. & Randolph, P. L. Porosity, Permeability, And Pore Structure of the Tight Mesaverde Sandstone, Piceance Basin, Colorado. *SPE Form. Eval.* **2**, 129–136 (1987).
3. Adebayo, A. R., Babalola, L., Hussaini, S. R., Alqubalee, A. & Babu, R. S. Insight into the pore characteristics of a Saudi Arabian tight gas sand

reservoir. *Energies* **12**, (2019).

4. Luffel, D. L. & Howard, W. E. Reliability of laboratory measurement of porosity in tight gas sands. *SPE Form. Eval.* **3**, (1988).
5. Sondergeld, C. H., Newsham, K. E., Comisky, J. T., Rice, M. C. & Rai, C. S. Petrophysical considerations in evaluating and producing shale gas resources. in *Society of Petroleum Engineers - Canadian Unconventional Resources and International Petroleum Conference 2010* vol. 1 (2010).
6. Song, L., Warner, T. & Carr, T. An efficient, consistent, and trackable method to quantify organic matter–hosted porosity from ion-milled scanning electron microscope images of mudrock gas reservoirs. *Am. Assoc. Pet. Geol. Bull.* **103**, (2019).
7. Sullivan, M. & Song, L. Briggs colour cubing of spectral gamma ray - A novel technique for easier stratigraphic correlation and rock typing. in *SPWLA 58th Annual Logging Symposium 2017* (2017).
8. Archie, G. E. The electrical resistivity log as an aid in determining some reservoir characteristics. *Trans. AIME* **146**, 54–62 (1942).
9. W. O. Winsauer, H. M. Shearin, P. H. Masson, M. W. Resistivity of Brine-Saturated Sands in Relation to Pore Geometry. *Am. Assoc. Pet. Geol. Bull.* **36**, 253–277 (1952).
10. Waxman, M. H. & Smits, L. J. M. Electrical Conductivities in Oil-Bearing Shaly Sands. *SPE Repr. Ser.* **243**, 107–122 (2003).
11. Poupon A. & Leveaux J. Evaluation of water saturation in shaly formations. *Log Anal.* **12**, 3–8 (1971).
12. Simandoux, P. Measures dielectrique en milieu Poreux, ap_plication a measure de saturation en eau, etude des mas_sifs argileauxle. *Rev. Inst. Fr. Pet* 193–215 (1963).
13. Adebayo, A. R., Al-Yousef, H. Y. & Mahmoud, M. A. An investigation of the effect of CO2-brine-rock interaction on determination of Archie's saturation exponent for carbon dioxide evaluation in carbonate reservoirs. *J. Pet. Sci. Eng.* **133**, 665–676 (2015).
14. Faurissoux, P., Colombain, A., Pujol, G., Fraute, O. & Nicot, B. Ultra Fast Capilary Pressure and Resistivity Index Measurements (Ufpcri) Combining Centrifugation , Nmr Imaging , and Resistity Profiling. *SCA Int. Symp. Vienna* 1–12 (2017).
15. Fleury, M. Resistivity in Carbonates: New Insights. *Proc. - SPE Annu. Tech. Conf. Exhib.* 3321–3329 (2002) doi:10.2523/77719-ms.
16. Ward, J. S. & Morrow, N. R. Capillary Pressures And Gas Relative Permeabilities Of Low-Permeability Sandstone. *SPE Form. Eval.* **2**, 345–356 (1987).
17. Newsham, K. E., Rushing, J. A. & Lasswell, P. M. Use of Vapor Desorption Data to Characterize High Capillary Pressures in a Basin-Centered Gas Accumulation with Ultra-Low Connate Water Saturations. in *SPE Annual Technical Conference and Exhibition,* (Denver, Colorado, 2003). doi:10.2118/84596-ms.
18. Collins, R. E. *Flow of Fluids Through Porous Materials*. (The Petroleum Publishing Co., Tulsa, OK, 1976).
19. Calhoun, J. C., Lewis, M. & Newman, R. C. Experiments on the Capillary Properties of Porous Solids. *J. Pet. Technol.* **1**, 189–196 (1949).
20. Melrose, J. C. Use of water-vapor desorption data in the determination of capillary pressure at low water saturations. *SPE Reserv. Eng. (Society Pet. Eng.* **3**, 913–918 (1988).
21. Thomson, W. On the equilibrium of vapour at a curved surface of liquid. *London, Edinburgh, Dublin Philos. Mag. J. Sci.* **42**, 448–452 (1871).
22. Morrow, N. R. & Harris, C. C. Capillary Equilibrium in Porous Materials. *Soc. Pet. Eng. J.* **5**, 15–24 (1965).
23. Dernaika, M. R. Combined capillary pressure and resistivity index measurements in tight gas sands using vapor desorption method. in *Deep Gas Conference and Exhibition 2010, DGAS 2010* (2010). doi:10.2118/132097-ms.
24. Lasswell, P.M., and Rushing, J. A. Laboratory analysis of electrical rock properties and capillary pressure in tight gas sands with low water saturations. in *Canadian well logging Society* 16–22 (Canadian well logging society, 2005).
25. Xiao, L., Mao, Z. qiang, Li, G. ren & Jin, Y. Estimation of Saturation Exponent from Nuclear Magnetic Resonance (NMR) Logs in Low Permeability Reservoirs. *Appl. Magn. Reson.* **44**, 333–347 (2013).
26. Xiao, L., Shi, Y., Li, G., Guo, H. & Li, J. A method to predict the resistivity index for tight sandstone reservoirs from nuclear magnetic resonance data. *Am. Assoc. Pet. Geol. Bull.* **105**, 1009–1032 (2021).
27. Feng, C., Yang, Z., Feng, Z., Zhong, Y. & Ling, K. A novel method to estimate resistivity index of tight sandstone reservoirs using nuclear magnetic resonance logs. *J. Nat. Gas Sci. Eng.* **79**, (2020).
28. Guo, Y. *et al.* Saturation evaluation of tight sandstone in the Dayi structure, West Sichuan Depression. *Front. Earth Sci.* **11**, 1–14 (2023).
29. Gao, F. *et al.* Low Permeability Gas-Bearing Sandstone Reservoirs Characterization from Geophysical Well Logging Data: A Case Study of Pinghu Formation in KQT Region, East China Sea. *Processes* **11**, (2023).
30. Dacy, J. & Martin, P. Practical advances in core-based water saturation analysis of Shaly tight gas sands. *Petrophysics* **49**, 17–27 (2008).